Journal of Fluids and Structures 103 (2021) 103290

Contents lists available at ScienceDirect

Journal of Fluids and Structures

journal homepage: www.elsevier.com/locate/jfs

The relevance of recoil and free swimming in aquatic locomotion

Damiano Paniccia [a,*], Giorgio Graziani [a], Claudio Lugni [b,c,d], Renzo Piva [a]

[a] Department of Mechanical and Aerospace Engineering, University of Rome "La Sapienza", Via Eudossiana, 18 - 00184 Rome, Italy
[b] CNR-INM, Marine Technology Research Institute, Rome, Italy
[c] NTNU-AMOS, Center for Autonomous Marine Operation Systems, Trondheim, Norway
[d] Institute of Marine Hydrodynamics, Harbin Engineering University, Harbin, China

ARTICLE INFO

Article history:
Received 7 January 2021
Received in revised form 11 March 2021
Accepted 13 April 2021
Available online 26 April 2021

Keywords:
Aquatic locomotion
Free swimming
Fish propulsion
Recoil
Biological fluid dynamics

ABSTRACT

The study of the free swimming of undulating bodies in an otherwise quiescent fluid has always encountered serious difficulties for several reasons. When considering the full system, given by the body and the unbounded surrounding fluid, the absence of external forces leads to a subtle interaction problem dominated, at least at steady state conditions, by the equilibrium of strictly related internal forces, e.g. thrust and drag, under the forcing of a prescribed deformation. A major complication has been dictated by the recoil motion induced by the non linear interactions, which may find a quite natural solution when considering as unknowns the velocity components of the body center of mass. A simplified two-dimensional model in terms of impulse equations has been used and a fruitful separation of the main contributions due to added mass and to vorticity release is easily obtained. As main results we obtain either the mean locomotion speed and the oscillating recoil velocity components which have a large effect on the overall performance of free swimming. Several constrained gaits are considered to highlight the relevance of recoil for realizing graceful and efficient trajectories and to analyze its potential means for active control.

1. Introduction

The swimming of a deformable body in water, either fish or cetacean, has been studied since the beginning (see e.g. Bainbridge, 1958; Lighthill, 1960; Wu, 1961), by considering the body held in a fixed position under an incoming uniform stream, or tethered with an opposite velocity, to evaluate the performance at steady state conditions. This choice was considered the most favorable for the implementation of simplified mathematical models and instrumental for experimental techniques or for computational solutions. As a consequence, the prevailing attention at the time was given to the resulting thrust which leads, together with the expended power, to the evaluation of the well known Froude efficiency (see e.g. Lighthill, 1960), usually adopted for marine vehicles where the propulsive force is easily separated from the resistive one. Hence, apart from the assigned stream in the forward direction, the other body motions either lateral or angular, perceived as recoil motions, did receive in general a secondary interest or no interest at all. To the best of our knowledge, Lighthill was the first one, at the beginning of the 60s, to emphasize the importance of the recoil, induced by the fluid–body interactions. He did actually pursue, as primary objective of his elongated body theory, the evaluation of thrust and efficiency produced by the prescribed deformation, but he analyzed also the recoil motion as a required

* Corresponding author.
E-mail address: damiano.paniccia@uniroma1.it (D. Paniccia).

https://doi.org/10.1016/j.jfluidstructs.2021.103290

correction to satisfy the equilibrium equations. Subsequently, several numerical investigations (see e.g. Maertens et al., 2017) tried to determine by the same procedure the effects of the recoil motion on the overall performance.

Since the animal muscular contractions give rise only to a change of shape relative to the center of mass, the whole body motion including the recoil should be given primarily by the center of mass motion generated by the interaction with the surrounding fluid. To this aim, an approach more suitable for self-propelled swimming was suggested by Saffman (1967) and subsequently adopted in numerical simulations by Carling et al. (1998), Kern and Koumoutsakos (2006), Borazjani and Sotiropoulos (2010), Yang et al. (2008), among others. The free-swimming mode provides as unknowns of the problem the velocity components of the body center of mass under the action of the internal forces exchanged with the otherwise quiescent fluid. Along this line, the motion of a deformable body in an unbounded fluid domain and in the absence of external forces, is analyzed here by imposing the conservation of momentum and of its moment for the entire fluid–body system. The undulatory deformation is usually prescribed, so to conserve linear and angular momenta in the absence of fluid, while the kinematic variables for the body center of mass are obtained by solving the equilibrium equations. Namely, the mean forward velocity in the body frame gives the animal locomotion while the oscillatory angular and lateral velocities are identified as the recoil motions with a significant impact on the swimming performance. The oscillatory part of the forward velocity is also obtained, but, as recognized by many authors (Bale et al., 2014; Smits, 2019), it plays a minor role in most cases.

Recently, several contributions in experimental biology fostered the measurements of the center of mass position, in a frame moving with the mean forward velocity, as a tool for evaluating and comparing different species and different styles of swimming (see e.g. Lauder, 2015; Xiong and Lauder, 2014). Actually, the forward, lateral and angular oscillating velocity components (surge, sway and yaw) are easily obtained with the present model while heave, i.e. the motion in the third direction, is not so important in fish swimming. The numerical values of the oscillating velocities, properly treated by statistical tools, may reveal the main properties of the self propelled locomotion as a signature of the style of swimming.

Purpose of the paper is to define the role of the recoil for a self-propelled body under a prescribed deformation and a non linear interaction with the surrounding fluid. The motion of the body center of mass, in terms of locomotion speed and of oscillating recoil velocities, is the most natural quantity to evaluate. To reduce this subtle problem to its essential features, as suggested by Schultz and Webb (2002) and recently by Akoz et al. (2019), we consider a two-dimensional potential flow model with generation of non-diffusing vorticity and its release from the trailing edge. In this way the related numerical scheme is able to separate the contribution of potential and of vortical impulse, by highlighting their different roles in the time evolution of the unsteady solution. The identification of the added mass term may provide a useful key for a physical interpretation of unsteady phenomena (see e.g. Limacher et al., 2018) while the analysis of the wake evolution, essential to define the asymptotic value of the locomotion speed, allows for the calculation of the energy injected into the fluid (see e.g. Bale et al., 2014). For the well known difficulties to disentangle the internal forces, given by thrust and drag, the standard measures of the efficiency are not easily detectable and we adopt a suitable form of the cost of transport (see e.g. von Kármán and Gabrielli, 1950; Bale et al., 2014) to evaluate the efficiency of the different styles of swimming . Moreover, we discuss with particular care the oscillating velocity components of the center of mass which have a notable importance for understanding different swimming modes and related means for active control.

Among the numerical results, for a better evaluation of free swimming features we analyze in comparison, as originally proposed by Reid et al. (2012), the simulations of constrained motions which are representative of cases where some recoil reactions are prevented. To obtain constrained gaits by the present model it is convenient to annihilate either one or more velocity components in the body frame, among lateral motion and rotation. As a primary result, the efficiency, in terms of the cost of transport, is measured for each one of the above simulations to assess the free swimming performance for aquatic locomotion. A simple tool for the active control of swimming may be obtained by modifying the recoil reaction throughout a sudden variation of the shape. For instance, as suggested by Domenici et al. (2014), the sailfish is able to raise a vertical fin to reduce lateral and angular oscillations with the aim to stabilize the trajectory during a predator–prey interaction. We will see by a crude approximation that an increase of the related components of the fish added mass matrix, consistent with the sail raising, may be instrumental to implement the required pattern control.

2. Material and methods

2.1. Mathematical model

We study the motion of a two-dimensional deformable body within an infinite volume of initially quiescent fluid with constant density. Since no external forces or moments are applied to the fluid–body domain, the self-propelled motion is due to the body undulations. In other words the total linear and angular momenta are conserved for the whole domain, while the forces and moments exchanged between fluid and body appear as internal actions. To express the equations for the fluid–body dynamics we adopt the classical formulation in terms of potential and vortical impulses that overcomes the difficulties to treat an unbounded domain, as largely discussed in the literature (see e.g. Landau and Lifschitz, 1986; Wu et al., 2006), and avoids the evaluation of the pressure on the body contour. Through the impulse formulation we can emphasize the contribution of the acyclic (non circulatory) potential as well as the effects of both the free vorticity and the cyclic part of the bound vorticity. A detailed formulation, though focused on pure potential flow, is given by Kanso (2009) while the extension to generated and released vorticity (see also Eldredge, 2007) is briefly presented here.

The locomotion of the deformable body is obtained by coupling the dynamics of the body and of the surrounding fluid. If we consider the body–fluid system ($\mathcal{V}_b + \mathcal{V}_f$), in the absence of external forces and moments the linear and angular momenta are conserved as given by

$$\frac{d}{dt}\left[\int_{\mathcal{V}_b} \rho_b \, \mathbf{u}_b \, dV + \int_{\mathcal{V}_f} \rho \, \mathbf{u} \, dV\right] = 0 \tag{1}$$

$$\frac{d}{dt}\left[\int_{\mathcal{V}_b} \rho_b \, \mathbf{x} \times \mathbf{u}_b \, dV + \int_{\mathcal{V}_f} \rho \, \mathbf{x} \times \mathbf{u} \, dV\right] = 0 \tag{2}$$

where $(\rho_b, \mathbf{u}_b)$ and $(\rho, \mathbf{u})$ are the density and the velocity of body and fluid, respectively.

Since forces and moments are not required in the present procedure, we may neglect in the above Eqs. (1)–(2) the time differentiation which would otherwise lead to a subsequent integration to find the kinematics of the body. Hence, by assuming an initial condition of quiescent fluid, we obtain a very efficient solution.

The second term within the square brackets in (1) is the fluid impulse $\mathbf{p}$ which can be expressed, via a well known vector identity, by two contributions due to the field vorticity $\boldsymbol{\omega}$ and to the vortex sheet over the body surface (see e.g. Noca et al., 1999; Wu et al., 2006; Graziani and Bassanini, 2002):

$$\mathbf{p} = \rho\left[\int_{\mathcal{V}_f} \mathbf{x} \times \boldsymbol{\omega} \, dV \; + \int_{S_b} \mathbf{x} \times (\mathbf{n} \times \mathbf{u}) \, dS\right] \tag{3}$$

where S_b is the body contour, $\mathbf{n}$ is the normal vector to S_b pointing into the flow domain and $\mathbf{u}$ is here the limiting value of the fluid velocity on S_b.

Another vector identity, is used for the second integral in (2) yielding an expression for the angular momentum (positive anticlockwise) on the body. Here we consider the moment with respect to a given pole (to be specified later either as the origin of the ground reference frame or as the body center of mass), so $\mathbf{x}$ is the generic distance of the field point from the pole. The angular impulse $\boldsymbol{\pi}$ is defined as:

$$\boldsymbol{\pi} = -\frac{1}{2}\rho\left[\int_{\mathcal{V}_f} |x|^2 \boldsymbol{\omega} \, dV + \int_{S_b} |x|^2 (\mathbf{n} \times \mathbf{u}) \, dS\right] \tag{4}$$

The velocity field $\mathbf{u}$ is expressed through the Helmholtz decomposition as the sum of the acyclic component and of the vorticity related one (i.e. wake plus the cyclic part of the bound vortex sheet):

$$\mathbf{u} = \nabla\phi + \nabla \times \Psi = \nabla\phi + \mathbf{u}_w \tag{5}$$

where ϕ and Ψ are referred to as the scalar and the (solenoidal) vector potential, respectively. These are given by the solution of the Laplace/Poisson equation, subject to the impermeable boundary condition on S_b and to a vanishing velocity at infinity.

The fluid impulse $\mathbf{p}$ given by (3) can be expressed in terms of its potential and vortical components, $\mathbf{p}_\phi$ and $\mathbf{p}_v$ respectively, where $\mathbf{p}_v$ is defined by adding the contributions of the released vorticity $\boldsymbol{\omega}$ and of the cyclic part of the bound vorticity $\mathbf{n} \times \mathbf{u}_w$ on S_b:

$$\mathbf{p}_v = \rho\left[\int_{\mathcal{V}_f} \mathbf{x} \times \boldsymbol{\omega} \, dV \; + \int_{S_b} \mathbf{x} \times (\mathbf{n} \times \mathbf{u_w}) \, dS\right]$$

to follow Lighthill's concept of additional vorticity which is given by summing up the field vorticity to the bound vorticity minus its potential part (which is related to the added mass).

The acyclic potential contribution $\mathbf{p}_\phi$, via a renown vector identity, is given by:

$$\mathbf{p}_\phi = \int_{S_b} \mathbf{x} \times (\mathbf{n} \times \nabla\phi) \, dS = -\rho \int_{S_b} \phi \, \mathbf{n} \, dS \tag{6}$$

The expression for the angular momentum can be similarly obtained by separating the potential $\boldsymbol{\pi}_\phi$ and the vortical $\boldsymbol{\pi}_v$ impulses as:

$$\boldsymbol{\pi}_\phi = -\rho \int_{S_b} \phi \, \boldsymbol{x} \times \mathbf{n} \, dS \tag{7}$$

$$\boldsymbol{\pi}_v = -\frac{1}{2}\rho\left[\int_{\mathcal{V}_f} |x|^2 \boldsymbol{\omega} \, dV + \int_{S_b} |x|^2 (\mathbf{n} \times \mathbf{u}_w) \, dS\right] \tag{8}$$

To enforce the conservation of the total impulses, the linear and angular momenta of the body have to be evaluated. To this aim, the location of the body center of mass $\mathbf{x}_{cm}$ and its velocity are defined by:

$$\mathbf{x}_{cm} = \frac{1}{m_b}\int_{\mathcal{V}_b} \rho_b \mathbf{x}_b \, dV \qquad \mathbf{u}_{cm} = \frac{d}{dt}\mathbf{x}_{cm} = \frac{1}{m_b}\int_{\mathcal{V}_b} \rho_b \mathbf{u}_b \, dV \tag{9}$$

where m_b is the body mass. Consequently, Eq. (1) yields:

$$m_b \, \mathbf{u}_{cm} + \mathbf{p} = 0 \tag{10}$$

Similarly, the angular impulse is recast from Eq. (4) in terms of the distance $\mathbf{x}'$ measured from $\mathbf{x}_{cm}$ as $\pi' = (\boldsymbol{\pi} - \mathbf{x}_o \times \mathbf{p}) \cdot \mathbf{e}_3$ where $\mathbf{x}_o$ is a given reference point. Hence, the angular momentum balance reduces to:

$$I_{zz} \, \Omega + \pi' = 0 \tag{11}$$

where I_{zz} is the moment of inertia with respect to the center of mass and Ω is the angular velocity.

The self-propelled motion of the body is described by the above reported Eqs. (10) and (11) in terms of $\mathbf{u}_{cm}$ and Ω which provide the locomotion speed and the recoil oscillating motions.

By using a Cartesian inertial frame $(\mathbf{e}_1, \mathbf{e}_2, \mathbf{e}_3)$, the body motion occurs in the plane $(\mathbf{e}_1, \mathbf{e}_2)$ and its translation is given by: $\mathbf{x}_o = x_o \, \mathbf{e}_1 + y_o \, \mathbf{e}_2$. Moreover, the body may undergo a rotation θ about the axis $\mathbf{e}_3$.

The motion of the body can be expressed as the sum of the prescribed deformation (shape variations with velocity $\mathbf{u}_{sh}$) plus the motion (with translational, $\mathbf{u}_{cm}$, and angular, $\boldsymbol{\Omega}$, velocities) of the center of mass (cm) reference frame. In the ground fixed inertial frame the angular velocity is $\boldsymbol{\Omega} = \dot{\theta} \, \mathbf{e}_3 \equiv \Omega \, \mathbf{e}_3$. The linear velocity is $\mathbf{u}_{cm} = \dot{x}_o \mathbf{e}_1 + \dot{y}_o \mathbf{e}_2$. Thus we can express the body motion as:

$$\mathbf{u}_b = \mathbf{u}_{sh} + \mathbf{u}_{cm} + \boldsymbol{\Omega} \times \mathbf{x}' \tag{12}$$

where $\mathbf{x}'$ is the position vector in the body reference frame, i.e.: $\mathbf{x} = \mathbf{x}_{cm} + \mathbf{x}'$. If Eq. (12) holds, the prescribed deformation has to satisfy:

$$\int_{\mathcal{V}_b} \rho_b \mathbf{u}_{sh} \, dV = 0 \qquad \int_{\mathcal{V}_b} \rho_b \mathbf{x}' \times \mathbf{u}_{sh} \, dV = 0 \tag{13}$$

Many authors (see e.g. Lighthill, 1970; Borazjani and Sotiropoulos, 2008; Reid et al., 2012; Maertens et al., 2017) adopt a generic deformation $\overline{\mathbf{u}}_{sh}$ which does not generally satisfy Eqs. (13), leading to

$$\int_{\mathcal{V}_b} \rho_b \overline{\mathbf{u}}_{sh} \, dV = m_b \boldsymbol{u}_o \qquad \int_{\mathcal{V}_b} \rho_b (\mathbf{x}' \times \overline{\mathbf{u}}_{sh}) \cdot \mathbf{e}_3 \, dV = I_{zz} \Omega_o \tag{14}$$

In this case to maintain our approach, the rigid motions given by $\boldsymbol{u}_o$ and Ω_o have to be removed since they should not be imposed on the self-propelled body as deeply analyzed by Bhalla et al. (2013) (see also Singh and Pedley, 2008).

The scalar potential ϕ introduced by the Helmholtz decomposition is further divided as $\phi = \phi_{sh} + \phi_{loc}$, where ϕ_{sh} is given by the imposed deformation velocity $\mathbf{u}_{sh}$ and ϕ_{loc} is given by the combination of the locomotion linear and angular velocity $\mathbf{u}_{cm}$ and Ω, according to the related boundary conditions on S_b

$$\frac{\partial \phi_{sh}}{\partial n} = \boldsymbol{u}_{sh} \cdot \boldsymbol{n} \qquad \frac{\partial \phi_{loc}}{\partial n} = (\boldsymbol{u}_{cm} + \boldsymbol{\Omega} \times \boldsymbol{x}') \cdot \boldsymbol{n}$$

A similar decomposition holds for both the linear and the angular impulses, i.e. $\boldsymbol{p}_\phi = \boldsymbol{p}_{sh} + \boldsymbol{p}_{loc}$ and $\pi'_\phi = \pi'_{sh} + \pi'_{loc}$. Finally, the locomotion impulses, $\boldsymbol{p}_{loc}$ and π'_{loc}, can be expressed in terms of the added mass coefficients reported in the classical treatises (see e.g. Lamb, 1975). For a body motion given by $\boldsymbol{u}_{cm}$ and Ω, we consider the Kirchhoff base potentials Φ_j to express $\phi_{loc} = u_{cm1}\Phi_1 + u_{cm2}\Phi_2 + \Omega\Phi_3$. When this decomposition is combined with the linear and angular fluid potential impulses, the relevant added mass coefficients m_{ij} appear in the equations of motion.

2.2. Solution procedure

To compute the numerical solution it is convenient to write the locomotion equations in a coordinate frame attached to the body. For the 2D problem under investigation, we consider the ground fixed frame $\{\mathbf{e}_1, \mathbf{e}_2, \mathbf{e}_3\}$ and the body frame $\{\mathbf{b}_1, \mathbf{b}_2, \mathbf{b}_3\}$ whose origin is $\mathbf{x}_o \equiv \mathbf{x}_{cm}$ and $\mathbf{b}_3$ is parallel to $\mathbf{e}_3$. In this frame, the linear velocity $\mathbf{V}_{cm} = V_1 \, \mathbf{b}_1 + V_2 \, \mathbf{b}_2$ and the momenta $\mathbf{P}$ and Π are given by:

$$\mathbf{u}_{cm} = \mathbf{R}\mathbf{V}_{cm} \qquad \mathbf{p} = \mathbf{R}\mathbf{P} \qquad \pi' = \Pi \tag{15}$$

where $\mathbf{R}$ is the rotation matrix relating the inertial to the body frame. By starting from Eqs. (10) and (11) and by combining with the decompositions shown in the previous subsection for both potential and vortical impulses, we obtain the system of equations that yields the body motion:

$$\begin{cases} V_1 \, (m_{11} - m_b) + V_2 \, m_{12} + \Omega \, m_{13} = P_{sh1} + P_{v1} \\ V_1 \, m_{21} + V_2 \, (m_{22} - m_b) + \Omega \, m_{23} = P_{sh2} + P_{v2} \\ V_1 \, m_{31} + V_2 \, m_{32} + b\Omega \, (m_{33} - I_{zz}) = \Pi_{sh} + \Pi_v \end{cases} \tag{16}$$

Let us underline that the locomotion unknowns Ω, V_1 and V_2, appearing within the linear and angular impulses, remain on the l.h.s while all the known quantities are shifted to the r.h.s., leading to a well-posed system of equations very suitable for the numerical solutions. A more detailed description of the mathematical aspects supporting the overall procedure is given in Paniccia et al. (2021). The impulses Π_{sh} and $\mathbf{P}_{sh}$ are due to the body deformation, while Π_v and $\mathbf{P}_v$ are the vorticity related quantities. The terms appearing on the l.h.s. in Eq. (16) express the generalized added mass matrix which, together with the body inertial properties, give the coefficient matrix for the locomotion variables. The body mass m_b is assumed to be constant while I_{zz} and m_{ij} change in time according to the shape deformation. In the following, to be consistent with most of the literature on the subject, the velocity components are renamed as $U = -V_1$ and $V = V_2$.

To solve the system of Eqs. (16), we consider an accurate but simplified numerical procedure which does not involve vorticity diffusion (see also Akoz and Moored, 2018). The evaluation of both potential and vortical impulses can be obtained by the discretization of the body surface and by a suitable model for the release of the concentrated vortex sheet via a Kutta condition to mimic the presence of a vanishing viscosity. Let us mention briefly some of the techniques adopted for the numerical results. The linearity of the impulse equations enables to isolate and separate the contribution of the added mass which is correctly evaluated at each time-step and partly located on the l.h.s. driving to a well-posed system of equations.

The flow solution is obtained by using an unsteady potential code which is based on the approach of Hess and Smith (1967) approximating the body by a finite number of panels, each one with a specific source strength, but with a common circulation density. The impermeability condition on each panel together with a suitable unsteady Kutta condition are needed in order to evaluate the source strengths and the uniform circulation density γ. Moreover, according to Kelvin's theorem, any change in circulation about the airfoil results in the release of vorticity by a wake panel attached to the trailing edge (see Basu and Hancock, 1978). At each time step the released wake panel is lumped into a point vortex which is shed into the wake and advected downstream by the flow field. Finally, let us stress that the extension to vorticity diffusion would lead to a classical vortex method (see Chorin, 1973; Koumoutsakos et al., 1994) without substantially changing the adopted numerical procedure. By this extension it would be possible to consider also a release from smooth portions of the body as in the case of the leading edge vortex which plays a very important role in several unsteady maneuvers out of the scope of the present work.

2.3. Swimming kinematics

The swimming fish is represented by an undulating body with a chord length c equal to 1 m and whose shape at rest corresponds to a NACA0012 airfoil. The body undulates according to an artificially designed deformation more suitable for bio-mimetic applications, hereafter referred to as synthetic deformation. This deformation is obtained by assigning the slope β of the body mid-line by the following expression for a traveling wave of constant amplitude $d\beta$ (assumed as $\frac{\pi}{10}$ rad) and a wave number k related to a wavelength (assumed equal to c) along the curvilinear coordinate s

$$\beta(s,t) = d\beta \sin(ks - 2\pi f\, t) \tag{17}$$

where f is the frequency (assumed equal to $\frac{10}{2\pi}$ s^{-1}). The instantaneous coordinates of the airfoil mid-line in the body-fixed frame are obtained by integrating Eq. (17)

$$x_c(s,t) = \int_0^s \cos\left(\beta(s,t)\right)\, ds \tag{18a}$$

$$y_c(s,t) = \int_0^s \sin\left(\beta(s,t)\right)\, ds \tag{18b}$$

and the resulting configurations are shown in Fig. 1a.

This coordinates are properly corrected consistently with Eq. (13) by removing any rigid linear and angular displacements associated to the center of mass to obtain the mid-line configuration shown in Fig. 1b. Basically, the shape of the body is prescribed with respect to its center of mass and its principal axes of inertia. A further advantage of the synthetic deformation consists in the automatic compliance of the inextensibility condition expressed as

$$\left(\frac{\partial y_c}{\partial s}\right)^2 + \left(\frac{\partial x_c}{\partial s}\right)^2 = 1 \tag{19}$$

which ensures that the length of the body does not change during the motion. Different deformations, closely related to natural styles of swimming, e.g. carangiform and anguilliform, will be considered later for a comparative analysis.

3. Numerical results

3.1. The effects of motion constraints

As anticipated in the previous sections, we are interested in evaluating the effect of both lateral translation and rotation, i.e. the two most relevant recoil motions, accompanying the fish locomotion generated by its shape deformation. To this

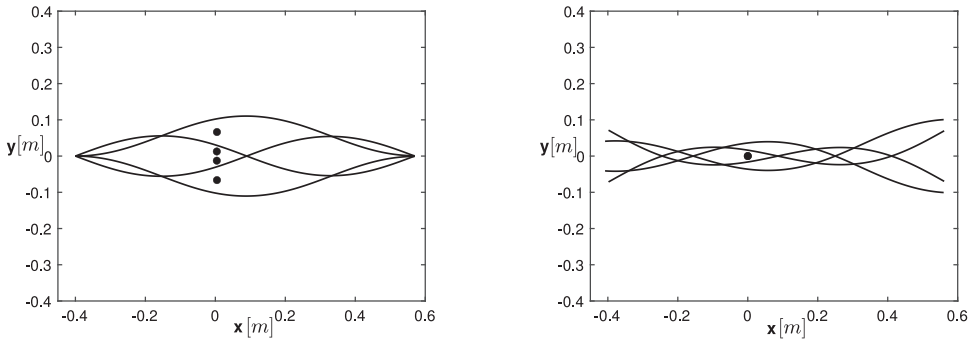

Fig. 1. (1a) Representative mid-line configurations obtained by the direct integration of Eqs. (17) giving an insight of their envelope– (1b) The same for the modified ones to satisfy Eq. (13). The dots represent the center of mass positions.

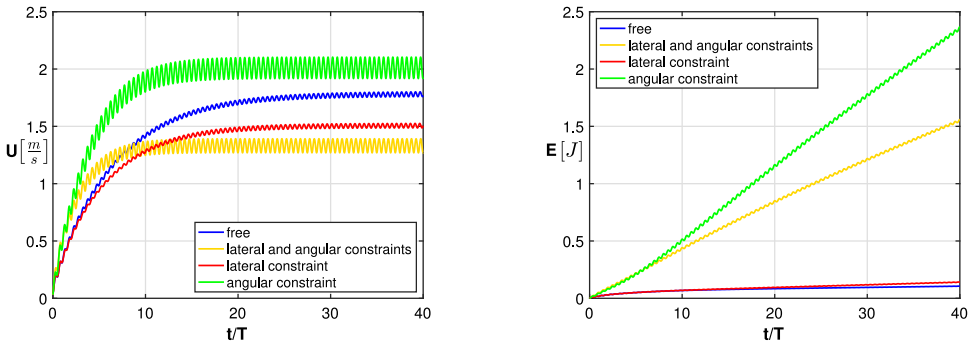

Fig. 2. Time history of (a) the forward velocity and (b) the kinetic energy for free swimming (blue) and constrained gaits: lateral and angular constraints (yellow), lateral constraint (red) and angular constraint (green). (For interpretation of the references to color in this figure legend, the reader is referred to the web version of this article.)

purpose, we consider the comparison between a fish whose recoil motions are allowed and a fish whose lateral and angular recoil motions in the body frame are prevented. This constrained gait implies that the center of mass of the fish is able to move exclusively along the forward direction as it occurs in many experimental investigations.Fig. 2a shows that, in these conditions (yellow curve), the body cannot reach the same asymptotic speed as in the free swimming case (blue curve). Correspondingly, the much larger energy consumption E shown in Fig. 2b, implies a larger cost of transport (COT), defined as the ratio between the mean rate of change of the energy $\overline{\dot{E}}$ and the mean forward velocity U_{loc} (see e.g. Bale et al., 2014; von Kármán and Gabrielli, 1950; Maertens et al., 2015). Consistently, for a certain steady state velocity, if such an unfavorable constraint is imposed, it follows an overestimation of the energy consumption. Let us mention that for the present model it is convenient to evaluate $\overline{\dot{E}}$ as the mean rate of change of the excess energy $\frac{1}{2}\int \boldsymbol{\Psi}\cdot\boldsymbol{\omega}\, dV$.

At this point, it is also interesting to analyze partial constraints which involve either the lateral or the angular motion while the forward oscillations are expected to have a minor impact on the swimming performance as claimed by many authors (see e.g. Maertens et al., 2017; Smits, 2019). When only the lateral motion is inhibited, the steady-state speed (red curve in Fig. 2a) is slightly lower than for free swimming (blue curve), while the energy consumption is still larger though almost comparable (same colors in Fig. 2b).

Instead, when only the angular motion is prevented, the velocity time history (green curve in Fig. 2a) shows a larger steady-state value together with a shorter transient. However, the energy consumption is even larger, as shown in Fig. 2b, when compared to the fully constrained case.

The bars shown in Fig. 3a represent the peak-to-peak oscillation of the forward, lateral and angular velocity components for the different constrained cases (see Xiong and Lauder, 2014).

It is interesting to note that the angular constrained case, characterized by the largest mean forward velocity, shows larger lateral oscillations to which, in general, is associated a larger thrust force in the forward direction. At the same time, the reduction of the locomotion speed associated with the lateral constraint may be a direct consequence of the suppression of lateral motion. The center of mass displacement is shown in Fig. 3b within a reference frame which moves

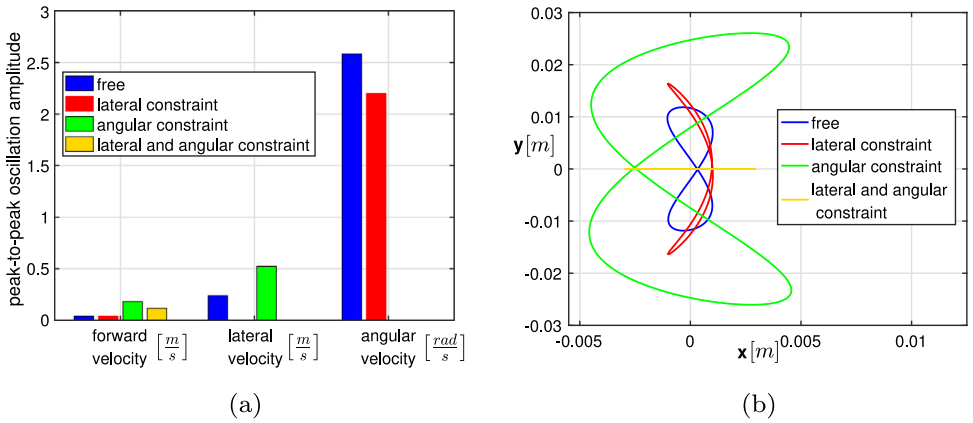

Fig. 3. (a) Amplitude of the peak-to-peak forward, lateral and angular velocity oscillations in the body frame. (b) Center of mass displacement in the locomotion frame for free (blue) and constrained motions: lateral and angular constraints (yellow), lateral constraint (red) and angular constraint (green). (For interpretation of the references to color in this figure legend, the reader is referred to the web version of this article.)

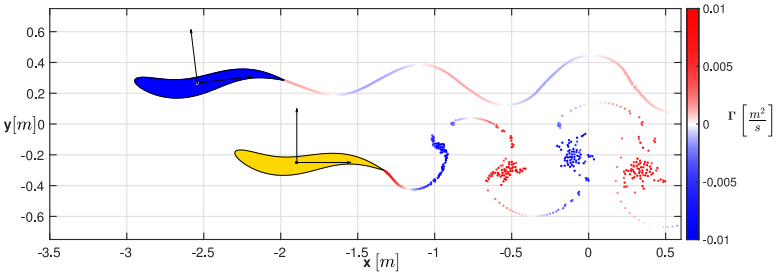

Fig. 4. Comparison at steady-state of the fully constrained (yellow) and the free swimming case (blue) - (animation-link). (For interpretation of the references to color in this figure legend, the reader is referred to the web version of this article.)

with the locomotion velocity, hereafter referred to as locomotion frame. We may notice that in this frame the lateral constrained case is characterized by an orthogonal motion with respect to the swimming direction which leads to a style of swimming quite close to the unconstrained one, as suggested also by the similar energy consumption in Fig. 2b (blue and red curves). Let us stress that large angular oscillations are present both in free swimming and in lateral constrained motions, together with a better energetic performance. Hence, we may consider the angular recoil as a primary form of control to optimize the center of mass trajectory. From the point of view of the expended energy, the lateral recoil motion does not seem as influential as the angular one.

To summarize, when only the lateral motion is constrained, the angular velocity is slightly lower than in free swimming while the associated energy consumption (see red curve in Fig. 2b) is almost the same. On the other hand, when the angular recoil motion is prevented, a huge increase in the energy consumption is observed (see green curve in Fig. 2b). Some of the phenomena related to constrained gaits are poorly intuitive hence, for a quick evaluation of the corresponding motions, we provide an animation (animation-link) with the direct comparison at steady-state of two quite different styles like the fully constrained (yellow case) and the free swimming one (blue case). For the sake of convenience a frame of the video is reported in Fig. 4. We may appreciate the larger speed of the free swimmer together with the stronger vortical wake for the constrained one corresponding to a much larger intensity of the released vortices whose circulation Γ is reported in Fig. 5. The impact of recoil on the swimming performance was also highlighted by other authors, starting from the preliminary work of Reid et al. (2012), limited to the lateral recoil motion, up to the work of Maertens et al. (2017) who clearly showed the importance of recoil for a correct estimation of the overall efficiency. On the same line of reasoning, Yang et al. (2008) reported much larger forces, hence larger power consumption, for the constrained case.

As a further deepening on these constrained motions, let us analyze how the potential and vortical impulses, as introduced in Section 2, cooperate to give the above presented results. To this purpose, we analyze both free swimming and fully constrained motion. We may observe in Fig. 6a how the potential contribution to the forward velocity reaches instantaneously a steady oscillatory state which is going to anticipate and guide the vortical contribution continuously growing in time together with release of new vortices. From the peak-to-peak oscillations shown in Fig. 6b, we may appreciate a larger value of the potential contribution for the constrained case while the value of the vortical one is quite comparable. Finally, a phase shift among the two contributions seems to be responsible for the significantly lower amplitude of the total velocity oscillations for free swimming. This result is confirmed by looking again at Fig. 2a and it seems clearly related to the lower circulation amplitude shown in Fig. 5.

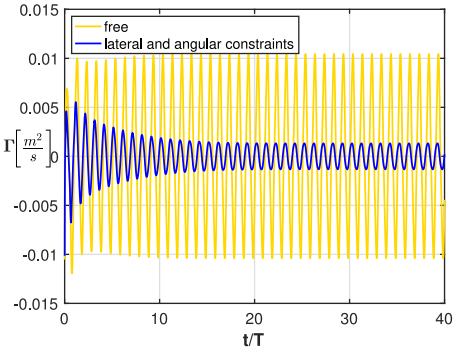

Fig. 5. Time history of the released circulation Γ for the fully constrained (yellow) and free swimming case (blue). (For interpretation of the references to color in this figure legend, the reader is referred to the web version of this article.)

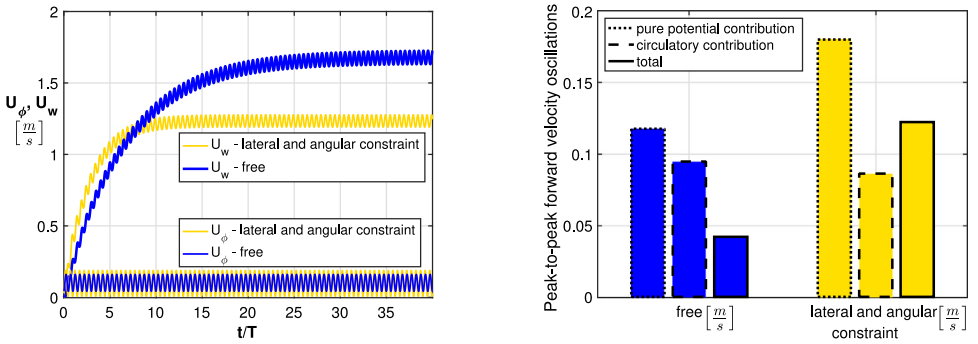

Fig. 6. (a) Time history of the forward velocity potential (U_ϕ) and circulatory (U_w) contributions for free swimming (blue) and fully constrained motion (yellow); (b) peak-to-peak oscillation for U_ϕ, U_w and the total velocity U. (For interpretation of the references to color in this figure legend, the reader is referred to the web version of this article.)

3.2. The impact of shape deformation

The above results has been obtained for the synthetic deformation to have a preliminary account of the constraints. However, in the literature, a large number of different approaches is used to describe different fish species. Most of them are based on analytical expressions for the lateral displacement of the mid-line obtained by fitting data from direct observations. These expressions usually consist of a traveling wave multiplied by a polynomial amplitude modulation $A(x) = ax^2 + bx + c$, whose coefficients are changed according to the fish swimming style. For an anguilliform swimmer, the amplitude modulation of the swimming motion is given by (Tytell and Lauder, 2004)

$$A(x) = 0.1 + 0.0323\,(x-1) + 0.0310\left(x^2-1\right) \tag{20}$$

For a carangiform swimmer, the amplitude modulation is given by (Videler and Hess, 1984)

$$A(x) = 0.1 - 0.0825\,(x-1) + 0.1625\left(x^2-1\right) \tag{21}$$

These prescribed swimming displacements are supposed to represent the real motions of the observed fishes. Nevertheless, in general, they do not satisfy the linear and angular momentum conservation and a recoil correction is required. It follows a substantial change of the final displacement as shown by Fig. 7, where it is possible to appreciate the differences between the prescribed mid-line envelopes and the modified ones accounting for the recoil, hence representing the whole motion. The synthetic deformation introduced here is also shown in the same figure to facilitate the comparison.

Despite the different prescribed deformations, once the recoil motions are considered, the three amplitude envelopes are quite similar, in particular with regard to the bottleneck near the center of mass. As a further strength for this analogy, the effects of constraints on the performance with the experimentally observed deformations are comparable to those discussed for the synthetic one. For instance, Fig. 8 summarizes the results obtained by constraining the anguilliform swimmer. No significant variation with respect to the synthetic deformation (see Fig. 2) appears if we exclude the mean asymptotic forward velocity reached in the case of the angular constraint, which in the present case almost coincides with the free swimming one. An even more significant comparison among the analyzed cases, (all with the same oscillation

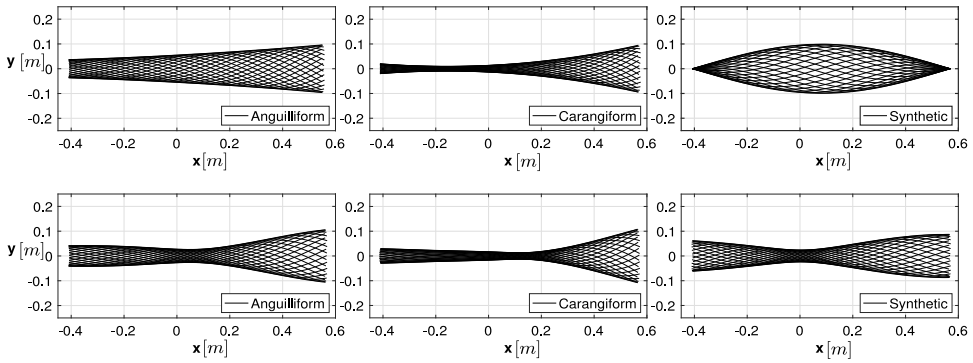

Fig. 7. Envelope of mid-line configurations for several prescribed deformations (top) and their corresponding recoil corrected displacement (bottom).

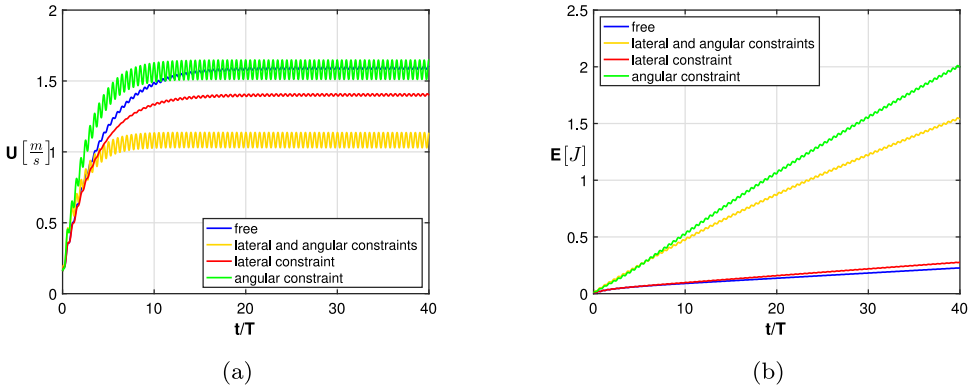

Fig. 8. Anguilliform (a) swimming velocity components and (b) fluid kinetic energy for free swimming (blue) and constrained gaits: lateral and angular constraints (yellow), lateral constraint (red) and angular constraint (green). (For interpretation of the references to color in this figure legend, the reader is referred to the web version of this article.)

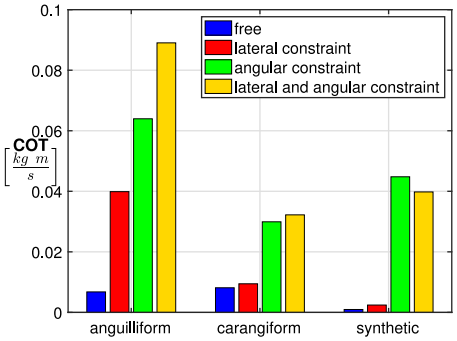

Fig. 9. Effects of constraints on the cost of transport for the analyzed different deformations for free swimming (blue) and constrained gaits: lateral and angular constraints (yellow), lateral constraint (red) and angular constraint (green). (For interpretation of the references to color in this figure legend, the reader is referred to the web version of this article.)

frequency and tail-beat amplitude) is given by the cost of transport whose increase (Fig. 9) is mostly affected by the angular constraint.

3.3. A tool for active control

The above reported constrained cases give, as a primary result, interesting information about the effect of the recoil motions on the swimming performance. At the same time, these constraints may represent also the limit case of an active control adopted by the fish through its appendages. For example, the sailfish, is well known to exploit the dorsal fin raising to optimize its performance during the predator–prey interactions. The dorsal fin, i.e. the sail, is kept retracted

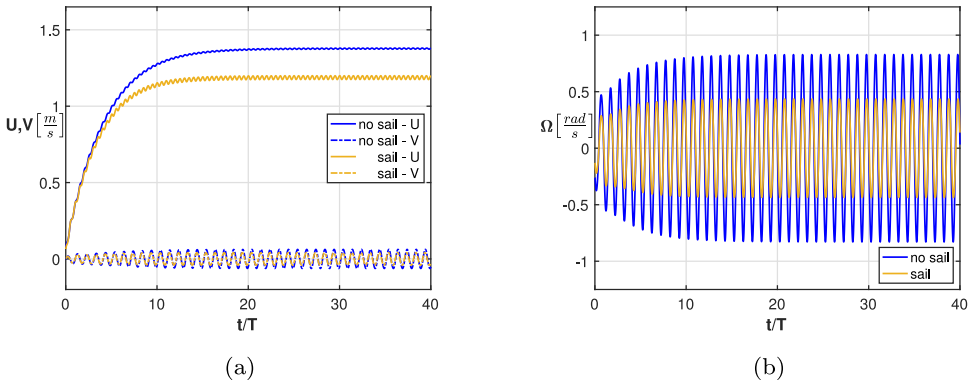

Fig. 10. Sailfish with (orange) and without (blue) the sail model: (a) forward, lateral and (b) angular velocity components. (For interpretation of the references to color in this figure legend, the reader is referred to the web version of this article.)

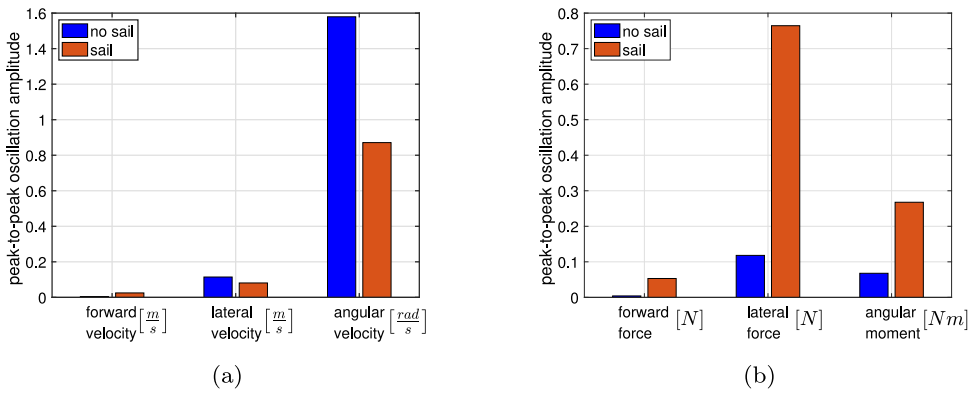

Fig. 11. Amplitude of the peak-to-peak oscillations for the sailfish: (a) forward, lateral and angular velocity and (b) forces and moment with (blue) and without (orange) the sail model. (For interpretation of the references to color in this figure legend, the reader is referred to the web version of this article.)

when cruising or fast swimming to avoid larger energy consumption, while it is extended to increase control during hunting maneuvers. On this subject, Domenici et al. (2014) deeply analyzed the behavior of the sailfish to show how the sail raising may be effective to reduce rotations and lateral translations. By approaching the schooling prey, the sailfish suddenly insert their long bill trying, in the mean time, to minimize any disturbance before slashing. Actually, when the sail is extended, the angular oscillations of the bill are reduced so as to make the bill a stealthy object, not easily detectable, while the approach velocity is reduced to match the prey swimming speed.

To reproduce the effect of the erected dorsal fin, we assumed, as a very crude approximation of a 3D extension, an extra value of the added mass consistent with a rigid flat plate (Faltinsen, 1993). The associated coefficients modify the body mass matrix to take into account the effects of the sail on the linear and angular velocity components.

As shown in Fig. 10, we obtain (as given by the experimental measurements by Domenici et al., 2014; Marras et al., 2015) either a lower swimming speed and the reduction of the angular and lateral oscillations. These are shown in a neat way in Fig. 11a, accompanied by an increase of both the moment and the lateral force experienced by the body (see Fig. 11b), since the larger inertance of the body due to the sail extension leads to a larger power consumption.

4. Final remarks

The locomotion of an undulating, neutrally buoyant, body has been studied either for the steady state and for the transient regime. Due to the involved complex phenomena, a simplified two-dimensional model has been adopted to obtain neat results as proposed by several authors (e.g. Schultz and Webb, 2002; Akoz and Moored, 2018; Akoz et al., 2019) and in a way encouraged by the midbody plane results obtained by Wolfgang et al. (1999) with a three-dimensional numerical model. Apart from the mean forward velocity representing the required locomotion, a particular attention has been given to the oscillating velocity components of the body center of mass which give the recoil motion originally introduced by Lighthill to satisfy the equilibrium equations of the free swimmer. The main points and related results discussed so far are here briefly summarized to highlight the most interesting findings about the relevance of recoil for free swimming performance:

- several constrained gaits have been considered to evaluate the importance of the various velocity components by inhibiting, either singly or jointly, their effect on the overall body motion;
- the locomotion velocity and the related expended energy clearly show the optimal performance of the free swimming with respect to all the considered constrained motions;
- the oscillating velocity components of the body center of mass, corresponding to the recoil motions, may be a simple and efficient tool, as recently proposed by experimental biologists, to understand and classify different styles of swimming;
- the attenuation of the recoil motions, on the other hand, may be seen as a suitable way to control several kinematic and dynamic aspects of the swimmer trajectory, as revealed by well known cases in nature;
- the most typical deformations proper of anguilliform and carangiform swimming styles are analyzed in comparison with the proposed synthetic deformation, with regard to the behavior in presence of recoil.

Some of the above statements, although based on simplified numerical results, give a valuable insight about the importance of recoil for the study of free swimming. Most of the results have been obtained for a synthetic shape deformation of particular interest for bio-mimetic applications and their assessment, through a systematic application to natural swimming styles, is requested. As a final comment, an extension of the methodology to account for vorticity diffusion (see e.g. Graziani et al., 1995; Eldredge, 2007) and for three-dimensional effects (see Wolfgang et al., 1999) should be implemented to deepen the analysis and to better understand further aspects of fish locomotion.

CRediT authorship contribution statement

Damiano Paniccia: Development of the manuscript, Conceptualization, Writing - review & editing. **Giorgio Graziani:** Development of the manuscript, Conceptualization, Writing - review & editing. **Claudio Lugni:** Development of the manuscript, Conceptualization, Writing - review & editing. **Renzo Piva:** Development of the manuscript, Conceptualization, Writing - review & editing.

Declaration of competing interest

The authors declare that they have no known competing financial interests or personal relationships that could have appeared to influence the work reported in this paper.

Acknowledgments

C.L. activity was partially supported by the Ministry of Science and Technology of P. R. China through Harbin Engineering University (G20190008061) and by the Research Council of Norway through the Centers of Excellence funding scheme AMOS, project number 223254. C.L. also acknowledges the Italian Ministry of Economic Development (MiSE) for the support under the Grant Agreement RdS PTR 2019–2021 - Tema 1.8: Energia elettrica dal mare.

Appendix A. Supplementary data

Supplementary material related to this article can be found online at https://doi.org/10.1016/j.jfluidstructs.2021.103290.

References

Akoz, E., Han, P., Liu, G., Dong, H., Moored, K.W., 2019. Large amplitude intermittent swimming in viscous and inviscid flows. AIAA J..
Akoz, E., Moored, K.W., 2018. Unsteady propulsion by an intermittent swimming gait. J. Fluid Mech. 834.
Bainbridge, R., 1958. The speed of swimming of fish as related to size and to the frequency and amplitude of the tail beat. J. Exp. Biol. 35.
Bale, R., Hao, M., Bhalla, A.P.S., Patankar, N.A., 2014. Energy efficiency and allometry of movement of swimming and flying animals. Proc. Natl. Acad. Sci. USA 111.
Basu, B.C., Hancock, G.J., 1978. The unsteady motion of a two-dimensional aerofoil in incompressible inviscid flow. J. Fluid Mech. 87.
Bhalla, A.P.S., Bale, R., Griffith, B.E., Patankar, N.A., 2013. A unified mathematical framework and an adaptive numerical method for fluid-structure interaction with rigid deforming and elastic bodies. J. Comput. Phys. 250.
Borazjani, I., Sotiropoulos, F., 2008. Numerical investigation of the hydrodynamics of carangiform swimming in the transitional and inertial flow regimes. J. Exp. Biol. 211.
Borazjani, I., Sotiropoulos, F., 2010. On the role of form and kinematics on the hydrodynamics of self-propelled body/caudal fin swimming. J. Exp. Biol. 213.
Carling, J., Williams, T.L., Bowtell, G., 1998. Self-propelled anguilliform swimming simultaneous solution of the two-dimensional Navier-Stokes equations and Newtons laws of motion. J. Exp. Biol. 201.
Chorin, A.J., 1973. Numerical study of slightly viscous flow. J. Fluid Mech. 57, 785–796.
Domenici, P., Wilson, A.D.M., Kurvers, R.H.J.M., Marras, S., Herbert-Read, J.E., Steffensen, J.F., Krause, S., Viblanc, P.E., Krause, P.C.J., 2014. How sailfish use their bills to capture schooling prey. Proc. R. Soc. B 281.
Eldredge, J.D., 2007. Numerical simulation of the fluid dynamics of 2D rigid body motion with the vortex particle method. J. Comput. Phys. 221 (2), 626–648.
Faltinsen, O., 1993. Sea Loads on Ships and Offshore Structures. Cambridge Univ. Press.

Graziani, G., Bassanini, P., 2002. Unsteady viscous flows about bodies: Vorticity release and forces. Meccanica 37.
Graziani, G., Ranucci, M., Piva, R., 1995. From a boundary integral formulation to a vortex method for viscous flows. Comput. Mech. 15.
Hess, J.L., Smith, A.M.O., 1967. Calculation of potential flow about arbitrary bodies. Prog. Aerosp. Sci. 8.
Kanso, E., 2009. Swimming due to transverse shape deformations. J. Fluid Mech. 631.
von Kármán, T., Gabrielli, G., 1950. What price speed? Specific power required for propulsion. Mech. Eng. 72, 775–781.
Kern, S., Koumoutsakos, P., 2006. Simulations of optimized anguilliform swimming. J. Exp. Biol. 209.
Koumoutsakos, P., Leonard, A., Pepin, F., 1994. Boundary conditions for viscous vortex methods. J. Comput. Phys. 113 (1), 52–61.
Lamb, H., 1975. Hydrodynamics, sixth ed. Cambridge Univ. Press.
Landau, L.D., Lifschitz, E.M., 1986. Fluid Mechanics, Vol. 6, second ed. Pergamon Press.
Lauder, G.V., 2015. Fish locomotion: Recent advances and new directions. Annu. Rev. Mar. Sci. 7.
Lighthill, J., 1960. Note on the swimming of slender fish. J. Fluid Mech. 9.
Lighthill, J., 1970. Aquatic animal propulsion of high hydromechanical efficiency. J. Fluid Mech. 44, 265–301.
Limacher, E., Morton, C., Wood, D., 2018. Generalized derivation of the added-mass and circulatory forces for viscous flows. Phys. Rev. Fluids 2.
Maertens, A.P., Gao, A., Triantafyllou, M.S., 2017. Optimal undulatory swimming for single fish-like body and for pair of interacting swimmers. J. Fluid Mech. 813.
Maertens, A.P., Triantafyllou, M.S., Yue, D.K.P., 2015. Efficiency of fish propulsion. Bioinspir. Biomim. 10.
Marras, S., Noda, T., Steffensen, J.F., Svendsen, M.B., Krause, J., Wilson, A.D., Kurvers, R.H., Herbert-Read, J., Boswell, K.M., Domenici, P., 2015. Not so fast: Swimming behavior of sailfish during predator–prey interactions using high-speed video and accelerometry. Integr. Comp. Biol. 55.
Noca, F., Shiels, D., Jeon, D., 1999. A comparison of methods for evaluating time-dependent fluid dynamic forces on bodies, using only velocity fields and their derivatives. J. Fluids Struct. 13.
Paniccia, D., Graziani, G., Lugni, C., Piva, R., 2021. On the role of added mass and vorticity release for self propelled aquatic locomotion. J. Fluid Mech. (in press).
Reid, D.A.P., Hildenbrandt, H., Padding, J.T., Hemelrijk, C.K., 2012. Fluid dynamics of moving fish in a two-dimensional multiparticle collision dynamics model. Phys. Rev. E 85.
Saffman, P.G., 1967. The self-propulsion of a deformable body in a perfect fluid. J. Fluid Mech. 28 (2).
Schultz, W.W., Webb, P.W., 2002. Power requirements of swimming: Do new methods resolve old questions?. Integr. Comp. Biol. 42.
Singh, K., Pedley, T.J., 2008. The hydrodynamics of flexible-body manoeuvres in swimming fish. Physica D 237, 2234–2239.
Smits, A.J., 2019. Undulatory and oscillatory swimming. J. Fluid Mech. 874.
Tytell, E.D., Lauder, G.V., 2004. The hydrodynamics of eel swimming: I wake structure. J. Exp. Biol. 207.
Videler, J., Hess, F., 1984. Fast continuous swimming of two pelagic predators saithe (pollachius virens): and mackerel (scomber scombrius). a kinematic analysis. J. Exp. Biol. 109.
Wolfgang, M.J., Anderson, J.M., Grosenbaugh, M.A., Yue, D.K.P., Triantafyllou, M.S., 1999. Near-body flow dynamics in swimming fish. J. Exp. Biol. 202.
Wu, T.Y., 1961. Swimming of a waving plate. J. Fluid Mech. 10.
Wu, J.Z., Ma, H.Y., Zhou, M.D., 2006. Vorticity and Vortex Dynamics. Springer.
Xiong, G., Lauder, G.V., 2014. Center of mass motion in swimming fish: effects of speed and locomotor mode during undulatory propulsion. Zoology 117.
Yang, Y., Wu, G.H., Yu, Y.L., Tong, B.G., 2008. Two-dimensional self-propelled fish motion in medium an integrated method for deforming body dynamics and unsteady fluid dynamics. Chin. Phys. Lett. 25.